World Academy of Science, Engineering and Technology
International Journal of Electronics and Communication Engineering
Vol:15, No:6, 2021

Evaluating the Feasibility of Magnetic Induction to Cross an Air-Water Boundary

Mark Watson, J.-F. Bousquet, Adam Forget

Abstract—A magnetic induction based underwater communication link is evaluated using an analytical model and a custom Finite-Difference Time-Domain (FDTD) simulation tool. The analytical model is based on the Sommerfeld integral, and a full-wave simulation tool evaluates Maxwell's equations using the FDTD method in cylindrical coordinates. The analytical model and FDTD simulation tool are then compared and used to predict the system performance for various transmitter depths and optimum frequencies of operation. To this end, the system bandwidth, signal to noise ratio, and the magnitude of the induced voltage are used to estimate the expected channel capacity. The models show that in seawater, a relatively low-power and small coils may be capable of obtaining a throughput of 40 to 300 kbps, for the case where a transmitter is at depths of 1 to 3 m and a receiver is at a height of 1 m.

Keywords—Magnetic Induction, FDTD, Underwater Communication, Sommerfeld.

I. Introduction

TRADITIONAL underwater communication technology includes the propagation of energy in the form of acoustic pressure waves as well as extremely low-frequency electromagnetic radiation. Although today's underwater communication systems are mature and robust, thye are based on acoustic energy propagation which is not able to transmit energy across the air-water interface. Extremely Low Frequency (ELF) electromagnetic radiation technology overcomes this problem; however, the size of the ELF antenna and the limited bandwidth makes this RF-based technology impractical for many applications such as subsea diver to surface communications, Internet of Underwater Things (IoUT) sensor networks, and Autonomous Underwater Vehicles (AUVs).

In [1], electric fields are generated underwater using a pair of electrodes. Experiments were conducted underwater with distances up to 5 m at frequencies between 100kHz and 6.35MHz. Using orthogonal frequency division multiplexing (OFDM), a low-power system was able to achieve throughput on the order of 10 Mbps, which is very promising; however, this does not address crossing of the air-water interface.

MIT's TARF system [2] addresses the need for a system capable of crossing the air-water interface; however, this technology is still in its infancy, and because of its reliance upon small perturbations on the water's surface caused by incident acoustic pressure waves, it is not immune to surface waves larger than just a few centimeters. Further, the TARF system is currently only capable of achieving a relatively low bandwidth ($\sim$400 bps).

In this paper, an analytical model of electromagnetic fields in a conductive half-space is used in conjunction with a custom Finite-Difference Time-Domain (FDTD) simulation tool to evaluate an underwater communication system based on the use a Magnetic Induction (MI) link.

This paper is organized as follows: in Section II, an analytical model of the MI link is presented based on the Sommerfeld integral; in Section III, the FDTD simulation tool is described; in Section IV, the analytical and FDTD models are evaluated for various system parameters; in Section V the channel capacity will be determined; and finally, in Section VI, conclusions are drawn.

Mark Watson, Jean Francois Bousquet, and Adam Forget are with the Department of Electrical and Computer Engineering, Dalhousie University, Halifax, NS, Canada (e-mail: mark.watson@dal.ca).

II. Magnetic Field Analytical Model

In this section, the Sommerfeld integral is presented to solve the magnetic field in non homogeneous media, as presented by Gibson in [3]. The numerical results of the magnetic field are converted to an induced voltage to allow a direct comparison with the output of the custom FDTD simulator developed in this work.

Based on the seminal work of Wait [4], Gibson presents an integral expression of the magnetic fields produced by a transmitting coil submerged in a good conductor at a receiver located above the air-water interface in a semi-infinite medium [3]. Simpler models exist in practice similar to that of Domingo [5] - where a transformer model is used to determine the MI link coupling loss - but Gibson's expression is derived directly from Maxwell's equations similar to that of [6] which makes it suitable for comparison with the FDTD simulations.

In Gibson's formulation, the magnetic field, $\vec{H}$, at a receiver placed at h meters above the sea surface is expressed in cylindrical coordinates as

$$\vec{H} = \frac{m_d}{2\pi h^3}\left[P\hat{\rho} + Q\hat{z}\right], \tag{1}$$

where symmetry about the azimuth, θ, is assumed, and m_d is the magnetic dipole moment given by $m_d = N_{Tx} I \pi r^3$. Also N_{Tx}, I, and r are the number of turns, maximum current in Amps, and radius of the transmitting coil in meters, respectively. The terms P and Q are found by evaluating the Sommerfeld integral defined as

$$(P, Q) = \int_0^\infty \frac{x^3 e^{-xZ}}{x+U} e^{-U}\left(J_1(xD), J_0(xD)\right) dx, \tag{2}$$

where $U^2 = x^2 + j2\left(h/\delta\right)^2$, and x is a dummy variable of integration arrived at through a change of variables to simplify the integral. Note that the distances $D = \rho/h$ and $Z = z/h$ are normalized with respect to h. Also, the skin depth, in meters, is defined as $\delta = \sqrt{1/\pi f \sigma}$, where f is the frequency of operation and σ is the conductivity of the media.

From (1), the induced voltage in the receiver coil can be estimated. From the definition of Faraday's law, $V_{emf} = -N_{Rx}\mu\frac{d}{dt}\iint_S \vec{H}\cdot d\vec{S}$, where N_{Rx} is the number of turns in the receiving coil. Then, if we assume $\vec{H}$ evaluated at the center of the receiving coil is nearly constant across the plane of the receiving antenna (with respect to the space variables), then the induced voltage can be estimated to be $V_{emf} \approx -N_{Rx}\mu\frac{d}{dt}\vec{H}\iint_S d\vec{S}$. Since $\iint_S d\vec{S}$ is just the surface area of the receiving antenna, πr^2, where r is the radius of the receiving coil, then the induced voltage can be approximated as $V_{emf} \approx -N_{Rx}\mu\frac{d}{dt}\pi r^2\vec{H}$. Taking the Fourier transform of this expression results in $V_{emf}\left(f\right) \approx -jN_{Rx}2f\mu\pi^2 r^2\vec{H}\left(f\right)$, and the magnitude of the induced voltage can be estimated as

$$|V_{emf}\left(f\right)| \approx N_{Rx}2f\mu\pi^2 r^2|\vec{H}\left(f\right)|. \tag{3}$$

Using the values for $|\vec{H}\left(f\right)|$ obtained by evaluating the Sommerfeld integral, a plot can be produced for $|V_{emf}\left(f\right)|$ which shows a decrease in the induced voltage at low frequencies and agrees with Faraday's law. Due to Faraday's law of induction at low frequencies and attenuation due to the conductivity of the water at high frequencies, the expected band-pass effect of the channel is visible in Fig. 1. With this, an optimal channel center frequency can be approximated as a function of the required range of transmission.

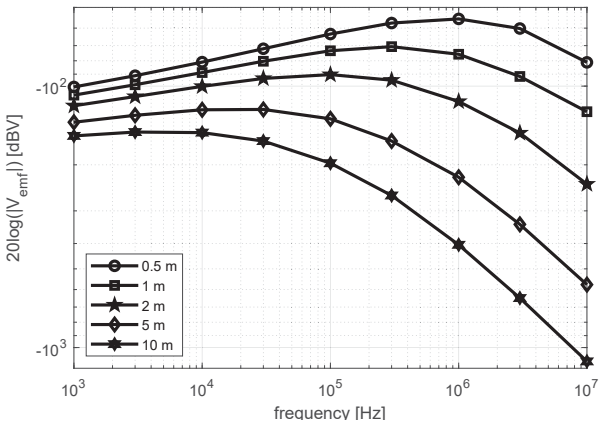

Fig. 1 Induced Voltage in Receiver Coil as a Function of Frequency and Distance based on Numerically Evaluating the Sommerfeld integral. Transmitter Depths Shown are 0.5, 1, 2, 5, and 10 Meters

III. FDTD Model

The simulation tool developed in this work is based on the Finite-Difference Time-Domain (FDTD) method. The simulation tool is intended to be highly configurable for different problems involving loop antennas, using either inductive coupling or radiation mechanisms. The FDTD model allows for a variety of input signals including pulses, single tones, and modulated signals. It provides an accurate representation of the user-defined properties of the medium and includes the effects of the input and output coils.

The simulation tool provides flexibility for the designer to choose the excitation to be a current source or a voltage source. For the latter, the voltage is converted to a current assuming a series RLC circuit. The RLC circuit has a quality factor of $Q = f_o/B = 2\pi L/R$, where f_o is the center frequency, and B represents the bandwidth of the coil. The quality factor fixes the maximum bandwidth of the communication system. The capacitor is automatically optimized for resonance, and the resistor value can be changed to control the coil current. Effectively, reducing the resistance increases the transmit power at the expense of bandwidth.

The transmitting coil current, I, is used to determine the magnetic fields, $\vec{H}$, encircling the coil wire using the integral form of Ampere's law. These magnetic fields are then used as a source and injected into the FDTD computational domain. Recall Ampere's law in integral form as

$$\oint_L \vec{H}\cdot d\vec{l} = I. \tag{4}$$

The FDTD channel model is a full-wave simulator based on Maxwell's equations. Recall that Faraday and Ampere's laws are, respectively

$$\nabla\times\vec{E} = -\mu\frac{\partial\vec{H}}{\partial t}, \tag{5}$$

$$\nabla\times\vec{H} = \sigma\vec{E} + \epsilon\frac{\partial\vec{E}}{\partial t}. \tag{6}$$

Since the problem geometry is 2D axial-symmetric about the z-axis, the FDTD simulation is formulated in cylindrical coordinates using a 2D geometry to decrease the computational time. As such, the TM mode is modelled in the (ρ, z) plane. The 2D Transverse Magnetic (TM) form of Maxwell's equations are shown in (7)-(9) in cylindrical coordinates and are the basis of the FDTD algorithm.

$$\frac{\partial E_\phi}{\partial z} = \mu\frac{\partial H_\rho}{\partial t} \tag{7}$$

$$\frac{1}{\rho}E_\phi + \frac{\partial E_\phi}{\partial \rho} = -\mu\frac{\partial H_z}{\partial t} \tag{8}$$

$$\frac{\partial H_\rho}{\partial z} - \frac{\partial H_z}{\partial \rho} = \sigma E_\phi + \epsilon\frac{\partial E_\phi}{\partial t} \tag{9}$$

where Δt is determined based on the Courant stability criterion [7], [8]. To solve the set of equations numerically, the domain is divided up into Yee cells [9] of size $\Delta\rho$ by Δz, where $\Delta\rho$ and Δz are determined based on either the smallest geometric feature or the smallest wavelength.

A Perfectly Matched Layer (PML) is implemented along the boundaries to minimize the reflection of electromagnetic energy back into the computational domain and to decrease the size of the simulation model and the computation time. The method used was described by Rumpf [10] and modified

for cylindrical coordinates. Using this PML, Faraday and Ampere's laws are modified such that $\nabla \times \vec{E} = -\mu [S] \partial \vec{H}/\partial t$ and $\nabla \times \vec{H} = \sigma \vec{E} + \epsilon [S] \partial \vec{E}/\partial t$. The term $[S]$ is introduced and represents an anisotropic tensor which matches the impedance of the interior of the computational domain with a fictitious lossy material at the boundary. $[S]$ is a 3rd rank tensor and expressed as

$$[S] = \begin{vmatrix} \frac{S_z S_\phi}{S_\rho} & 0 & 0 \\ 0 & \frac{S_\rho S_\phi}{S_z} & 0 \\ 0 & 0 & \frac{S_\rho S_z}{S_\phi} \end{vmatrix}, \tag{10}$$

where the matching condition used here is $S_i = 1 + \sigma_i / j2\pi f\epsilon$, and σ_i is equal to 0 S/m outside of the PML, while σ_i is equal to $(\epsilon_i / 2\Delta t)(i/l_i)^3$ S/m inside the PML, l_i is the length of the PML in meters, and $i = \rho$, ϕ, or z. The update equations shown in (7)-(9) are modified due to this term and can be found in [10].

Fig. 2 shows a screenshot of an animation generated by the FDTD simulator. The image on the left shows the entire computational domain with the colorbar representing $|H_z|$ scaled to ± 1 A/m. The image on the right shows the air-water interface and receiving coil scaled to ± 10 mA/m.

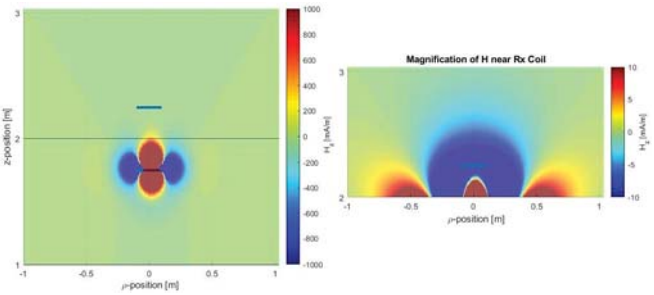

Fig. 2 Screenshot of FDTD Simulation. Tx Coil on Bottom, Rx Coil on Top. Image on Left: Full-Domain Scaled to ± 1 A/m With Region Separated by Line Indicating Air-Water Boundary. Image on Right: Close-up of Air-Water Interface Scaled to ± 10 mA/m With Only the Rx Coil Visible

Finally, the FDTD-based channel model is coupled to the receiving coil by utilizing Faraday's law shown defined as

$$V_{emf} = N_{Rx} \mu \frac{d}{dt} \iint_S \vec{H} \cdot d\vec{S}, \tag{11}$$

where the integral is evaluated numerically using the trapezoidal rule, and the surface area S is that of the receiving coil.

IV. Evaluation of the Two Models

This section will show key results of the analytical and FDTD models. The FDTD simulations were run with the receiver coil fixed horizontally at heights of 0.5 and 1 meter above the water's surface, while the transmitter is aligned horizontally and coaxial with the receiver, and at various transmitter depths. Note that the bottom half of the computational domain is water with a conductivity (σ) of 4 S/m (seawater) and a relative permittivity (ϵ_r) of 81, the top half is air, and the air-water interface is located at 1 m in the z-direction.

Wait's Sommerfeld integral was evaluated numerically using MATLAB's built-in *quad1()* function which uses adaptive Gauss/Lobatto quadrature [3]. A comparison of the results of these two models for the transmitter depths of 0.5, 1.0, 2.0, and 3.0 m and receiver heights of 0.5 and 1 m is shown in Fig. 3. The coils are assumed to have a 10 cm radius, the transmitting coil having 5 turns, the receiving coil having 5 turns, and the driving current has a maximum amplitude of 1 A to maintain the low-power requirement.

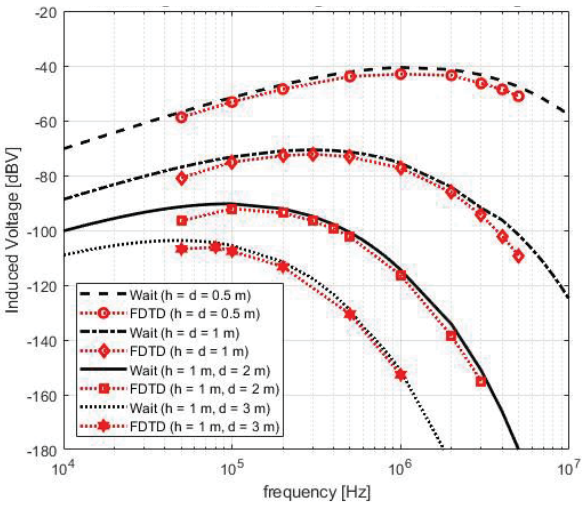

Fig. 3 Comparing the Predictions of the Induced Voltage in Receiver Coil Using Wait's Analytical Model and the FDTD Simulations as a Function of Frequency, Transmitter Depths (d), and Receiver Heights (h)

Fig. 3 shows a good match between the FDTD simulation results and Wait's analytical expression in terms of optimizing the center frequency for various coil configurations; however, the FDTD results deviate from the analytical model at the lower frequencies. The maximum induced voltage and optimum carrier frequencies are shown in Table I.

TABLE I
Comparing Results of Analytical and FDTD Models

Rx Height / Tx Depth	Analytical	FDTD
0.5 m / 0.5 m	-40.6 dBV / 1 MHz	-43.0 dBV / 1 MHz
1.0 m / 1.0 m	-70.6 dBV / 300 kHz	-72.2 dBV / 300 kHz
1.0 m / 2.0 m	-90.4 dBV / 100 kHz	-92.1 dBV / 100 kHz
1.0 m / 3.0 m	-103.7 dBV / 50 kHz	-106.2 dBV / 80 kHz

V. Evaluation of Channel Capacity

In this section, an expression for the channel capacity is presented based on predicted thermal and atmospheric noise conditions, and the voltage signal induced in the receiver.

It is recognized that atmospheric noise produces significant interference at low frequency. According to [3], the atmospheric noise temperature ratio F_a reaches several hundred dBs below 10 kHz, which is well below our frequency of interest. In this work, the contribution of the thermal noise voltage, $\sqrt{4kT_0BR}$ in the load resistance, R, at the receiver is added to the atmospheric noise, $\sqrt{4kT_0BF_aR_r}$, where R_r is

the radiation resistance. Note that k is Boltzmann's constant and T_0 is the ambient noise temperature. Also, the radiation resistance, R_r, of an electrically small loop antenna can be found in [11] and [12]; however, in this work, since the coil is small compared to the wavelength, radiation is not the main mechanism of energy transport, so R_r is assumed to be much smaller than R ($\sim$50 Ω).

To assess the channel capacity, the results of the analytical and FDTD models are used to determine the induced voltage, V_{emf}. To obtain the Signal-to-Noise Ratio (SNR) at the receiver, as described in [3], the induced voltage is used together with the thermal and atmospheric noise voltages. The SNR is expressed in its final form by

$$\mathrm{SNR} = \frac{V_{emf}}{\sqrt{4kT_0BR}} \Big/ \sqrt{1 + \frac{T_a R_r}{T_0 R}}, \tag{12}$$

where the expression used to estimate the channel capacity is the well-known Shannon's formula expressed by

$$C = B \cdot \log_2 (1 + \mathrm{SNR}). \tag{13}$$

From [13], Shannon's formula assumes an Additive White Gaussian Noise (AWGN) channel with no distortion, so this is considered a first-order approximation.

The system bandwidth is defined by the quality factor, Q, of the coils, such that $Q = f_o/B$. We impose the constraint $5 \leq Q \leq 10$ based on the lumped components of the RLC circuit. This limits the system bandwidth to 6 to 12 kHz.

Using (12) and (13), and the test parameters described above, the SNR and channel capacity was calculated from the data obtained from the FDTD model and are shown in Table II. The FDTD model shows theoretical channel capacities well above tens of kbps may be possible with transmitter depth up to a few meters. Of course, this is for the case where the two coils are aligned coaxially. The performance would be degraded if the coils were not aligned, but this scenario was not evaluated here.

TABLE II
DETERMINING SNR AND CAPACITY USING FDTD MODEL

Rx Height / Tx Depth	SNR [dB]	Capacity [kbps]
0.5 m / 0.5 m	85.6	1421.8
1.0 m / 1.0 m	61.6	307.1
1.0 m / 2.0 m	46.5	77.3
1.0 m / 3.0 m	33.4	44.6

VI. CONCLUSION

In conclusion, this work proposes a means to analyze and predict the performance of a high-speed underwater communication link which utilizes magnetic induction to cross the air-water boundary. A procedure is developed to assess the capacity of the MI link utilizing the results of the analytic and FDTD models, within constraints imposed by the hardware implementation of a test platform. With transmitter depths from 1 to 3 meters and a receiver height of 1 meter, the analytical model and FDTD simulation tool are used to determine the optimum carrier frequencies at each depth with channel capacities ranging from 40 to 300 kbps. These results show magnetic induction has excellent potential to provide a means of relatively low-power, compact, and high-speed data transmission across an air-water interface at shallow depths.

ACKNOWLEDGMENT

This work has been sponsored by an NSERC Collaborative Research and Development fund, in partnership with Ultra Electronics Maritime Systems.

REFERENCES

[1] A. Zoksimovski, D. Sexton, M. Stojanovic, and C. Rappaport, "Underwater electromagnetic communications using conduction - channel characterization," *Ad Hoc Netw.*, vol. 34, no. C, p. 42–51, Nov. 2015. [Online]. Available: https://doi.org/10.1016/j.adhoc.2015.01.017

[2] F. Tonolini and F. Adib, "Networking across boundaries: Enabling wireless communication through the water-air interface," in *ACM SIGCOMM 2018 Confrence*, ser. SIGCOMM '18. New York, NY, USA: ACM, 2018. [Online]. Available: http://doi.org/10.1145/3230543.3230580

[3] D. Gibson, *Channel Characterisation and System Design for Sub-Surface Communications*. Leeds, Great Britain: Lulu Enterprises, 2010.

[4] J. R. Wait, "Electromagnetic fields of sources in lossy media," in *Antenna Theory - Part 2*. McGraw-Hill, 1969, pp. 468–471.

[5] M. Domingo, "Magnetic induction for underwater wireless communication networks," *IEEE Trans. Antennas Propag.*, vol. 60, no. 6, pp. 2929–2939, 2012.

[6] H. Guo, Z. Sun, and P. Wang, "Multiple Frequency Band Channel Modeling and Analysis for Magnetic Induction Communication in Practical Underwater Environments," *IEEE Transactions on Vehicular Technology*, vol. PP, no. 99, pp. 1–1, 2017.

[7] S. Taflove, A. Hagness, *Computational Electrodynamics: The Finite-Difference Time-Domain Method*, 3rd ed. Boston, Massachusetts: Artech House, 2005.

[8] M. N. O. Sadiku, *Numerical Techniques in Electromagnetics with MATLAB*, 3rd ed. Boca Raton, Florida: CRC Press, 2015.

[9] K. S. Yee, "Numerical solution of initial boundary value problems involving maxwell's equations in isotropic media," *IEEE Transactions on Antennas and Propagation*, vol. 14, pp. 302–307, 1966.

[10] R. C. Rumpf, "Electromagnetic analysis using finite-difference time-domain," University of Texas at El Paso, available: https://empossible.net/academics/emp5304, Last accessed 03 March 2020.

[11] W. Stutzman and G. Thiele, *Antenna Theory and Design*, ser. Antenna Theory and Design. Wiley, 2012. [Online]. Available: https://books.google.ca/books?id=xhZRA1K57wIC

[12] C. A. Balanis, *Antenna Theory: Analysis and Design*, 4th ed. Hoboken, New Jersey: Wiley, 2016.

[13] Z. Lathi, B. P. Ding, *Modern Digital and Analog Communication Systems*, 5th ed. New York, New York: Oxford University Press, 2019.